ACS APPLIED ELECTRONIC MATERIALS

pubs.acs.org/acsaelm Article

# Realizing Low-Temperature Charge-Transfer-Type Insulating Ground State in Strained $V_2O_3$ Thin Film

Sophia Sahoo, Anupam Jana, Anita Bagri, Supriyo Majumder, Parasmani Rajput, Shambhu Nath Jha, Frank M. F. de Groot, Ram Janay Choudhary,* and Deodatta Moreshwar Phase

Cite This: *ACS Appl. Electron. Mater.* 2022, 4, 3036−3048 Read Online

ACCESS | Metrics & More | Article Recommendations

**ABSTRACT:** Controlling the electronic properties of strongly correlated systems, observing electron−electron correlation-driven metal to insulator transition (MIT) is a key point for the next-generation solid-state Mottronic devices. Thus, the knowledge of the exact nature of the insulating state is an essential need to enhance the functionality of the material. Therefore, we have investigated the electronic nature of the insulating state of a classical Mott insulator $V_2O_3$ thin film (epitaxial) using low-temperature (LT) (120 K) resonant photoemission spectroscopy and X-ray absorption near-edge spectroscopy measurements. Temperature-dependent valence band spectra (VBS) reflect the transfer of spectral weight from the metallic coherent band ($A_M$) near the Fermi level ($E_F$) to the insulating Mott−Hubbard screened band ($C_I$) at a binding energy of around 2.4 eV. Such a transfer of spectral weight upon MIT leads to vanishing of the density of states at $E_F$ and opens a band gap. The strong presence of the $3d^n\underline{L}$ final state is observed near the $E_F$ of LT VBS, confirming the presence of an O 2p band participating in low-energy charge fluctuation. This study further endorses the charge-transfer (CT)-type ($U > \Delta$) insulating nature of a strained $V_2O_3$ thin film at LT, unlike its bulk counterpart, which is placed intermediate ($U-\Delta$) between the CT and the Mott−Hubbard regime. Modifying the electronic ground state of $V_2O_3$ to the CT nature via the epitaxial strain in thin films provides a way to tailor the electronic energetics, with its implications to next-generation correlation-derived switching devices.

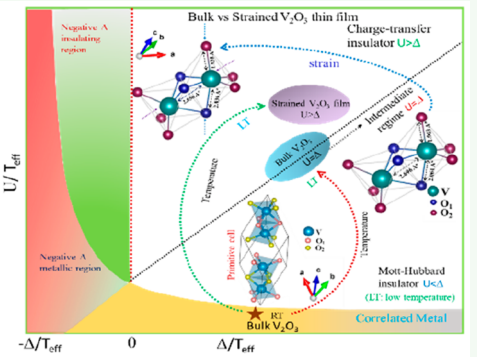


**KEYWORDS:** *epitaxial thin film, metal to insulator transition, strongly correlated system, Mottronics, X-ray absorption spectroscopy, resonant photoemission spectroscopy*



## INTRODUCTION

The competition between localization due to on-site Coulomb correlation and the itinerant behavior of electrons plays a crucial role in determining the complex and fascinating properties of strongly correlated systems.[1] The presence of various competing interactions resulting from charge, spin, orbital, and lattice degrees of freedom can lead to many exotic properties including high-temperature superconductors,[2] metal to insulator transition (MIT),[3] colossal magnetoresistance,[4] and so on. Vanadium-based compounds often reveal Mott MIT transition and represent a class of quantum materials exhibiting the most promising functionalities for the investigation of electrode materials for emerging metal-ion batteries,[5−7] emerging electrochemical energy storage,[8] and neuromorphic circuits.[9] Among these oxides, vanadium sesquioxide ($V_2O_3$), often considered as a prototype Mott−Hubbard (M−H) system, is one of the most remarkable examples in correlated oxide systems.[10] $V_2O_3$ presents a rich phase diagram as a function of temperature, pressure, or doping and undergoes a first-order transition at around 150 K from a rhombohedral paramagnetic metal (PM) phase to the monoclinic antiferromagnetic insulating (AFI) phase.[11] It crystallizes in the corundum structure, with four vanadium atoms in the primitive unit cell at ambient temperature and pressure. The V cations are surrounded by a distorted octahedron of $O^{2-}$ ions. Due to the electrostatic interaction of V 3d electrons with the surrounding oxygen ions, the fivefold degenerate V 3d levels undergo crystal-field splitting into a low-lying triplet $t_{2g}$ and upper-lying doublet $e_g$ energy states. In $V_2O_3$, the low-lying $t_{2g}$ orbitals accommodate two electrons in each $V^{3+}$ ion. A small trigonal distortion along the *c*-axis further splits the $t_{2g}$ level into doubly degenerate $e_g^{\pi}$ and non-degenerate $a_{1g}$ levels.[12] An energy gap of ∼0.6 eV opens between $e_g^{\pi}$ and $a_{1g}$ across the PM to AFI transition,[13] with a huge enhancement in electrical resistivity.[14] Earlier studies

Received: April 8, 2022
Accepted: May 30, 2022
Published: June 13, 2022

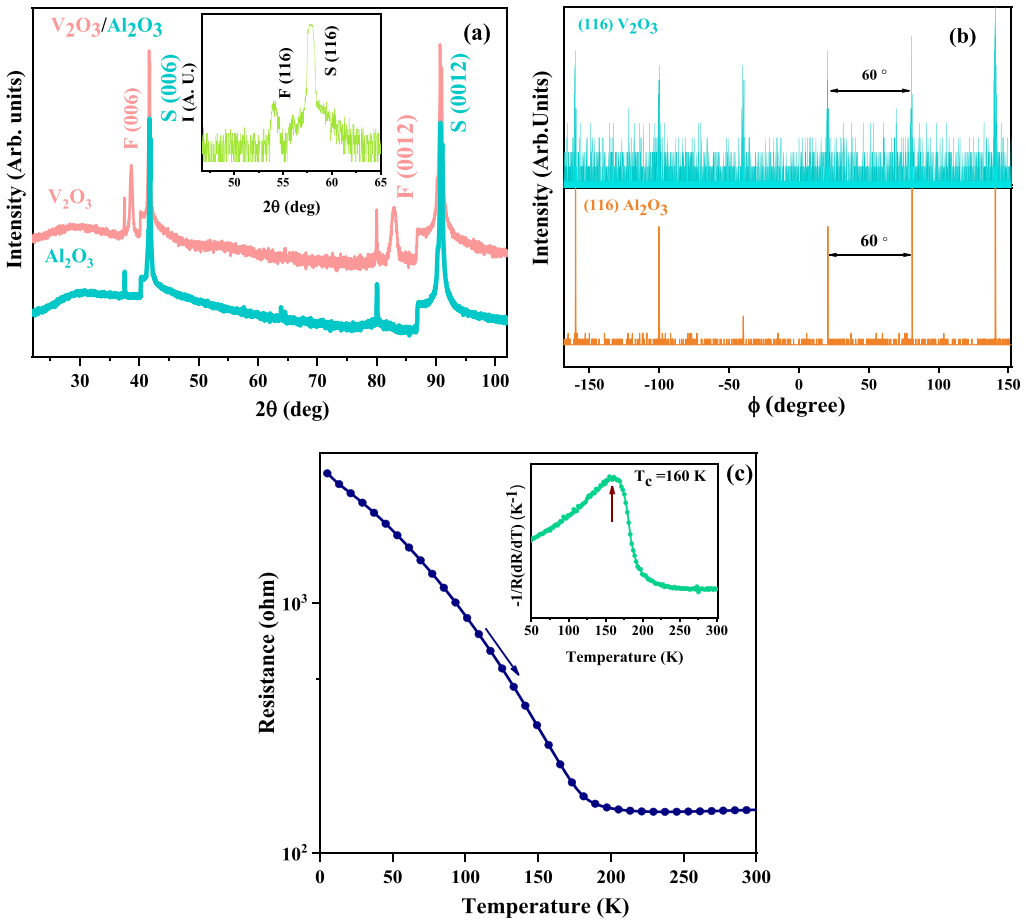


**Figure 1.** Structural characterizations of the $V_2O_3$ thin film. (a) Room temperature $\theta-2\theta$ out-of-plane XRD pattern of the $V_2O_3$ thin film grown on a (001)-oriented $Al_2O_3$ substrate (inset shows the in-plane $\theta-2\theta$ XRD of the $V_2O_3$ thin film) and (b) in-plane $\varphi$ scans recorded along the (116) direction of the $Al_2O_3$ substrate and $V_2O_3$ thin film at room temperature. (c) Temperature-dependent resistivity of the $V_2O_3$ thin film (warming cycle): Upper inset shows the resistance derivative with respect to temperature.

suggest that the electrical transport properties are highly sensitive to external perturbations such as epitaxial strain, hydrostatic pressure, chemical doping, and so on.[15,16] Moreover, using pressure and chemical doping in $V_2O_3$, MIT could be tuned from the iso-structural paramagnetic metal to the paramagnetic insulator (PI) phase.[17−19] Recently, Hu et al. demonstrated the evolution of MIT with trigonal distortion or, equivalently, the alteration in the c/a ratio in the $V_2O_3$ thin film.[20] Controlling the epitaxial strain, Homm et al. established a room temperature (RT) Mott-MIT in Cr-doped and pure $V_2O_3$ films.[21] Hence, controlling the electronic properties of $V_2O_3$ that feature an MIT is a key requirement that offered a new approach for developing a new class of electronics "Mottronics".

Electrical and magnetic properties of $V_2O_3$ can be best explained from its electronic structure. Using the molecular-orbital model,[22] Goodenough suggested three symmetries for the V 3d band and describes the electronic structure of $V_2O_3$. Also, the monoclinic distortion in the insulating phase (I-phase) causes the abrupt expansion of the V−V bond length in the V ion pair and rotation of the V−V bond direction by about 1.8° from the *c*-axis that is with respect to the basal plane. As a result, the oxygen octahedra surrounding the V pairs are skewed. Across the MIT, the $a_{1g}$ bands are shifted up in energy and the exchange split $e_g^{\pi}$ bands form the lower Hubbard band (LHB) and upper Hubbard band (UHB). The dynamical mean-field theory (DMFT) predicts the coexistence of coherent quasi-particle (QP) features close to the $E_F$ and incoherent LHB at a higher binding energy ($E_B$), which characterizes the correlated metallic phase (M-phase) of the M−H compound.[23]

In consequence of electron correlation effects, $V_2O_3$ possesses several technological applications such as in electrical and optical switching devices,[24] light detectors, and critical temperature sensors.[25] Recently, the $V_2O_3$ film has been explored as a voltage-controlled Mott device,[26] and efforts are devoted to achieving complete control of the electronic phase transformation for non-volatile resistive-switching devices.[27] Both thermal and nonthermal resistive switching can be explained in terms of LHB and UHB.[28] Hence, the electronic origin of these bands participating in the switching phenomena should be studied in detail. For such device applications and efficient functionalities, it is extremely important to realize the competing energetics such as on-site d−d Coulomb repulsion energy *U*, the charge transfer (CT) energy Δ, bandwidth (*W*), crystal-field splitting, ligand p-metal d hybridization energy $T_\sigma$ along with the nature of the insulating state.[1] However, early transition metal (TM) (Sc−Cr) compounds have been placed in the M−H regime ($U < \Delta$) in contrast to the late TM compounds, which mainly fall in the CT regime ($U > \Delta$).[29] In the M−H insulating state, the lowest-energy charge fluctuation across $E_F$ is governed between the dominated TM 3d states,


https://doi.org/10.1021/acsaelm.2c00460
ACS Appl. Electron. Mater. 2022, 4, 3036−3048

and the energy difference between the LHB and UHB defines the energy gap of the system, while in a CT insulator, the lowest energy charge fluctuation is mainly dominated by the mixed V 3d−O 2p state and UHB. Based on cluster model calculations,[30] previous studies suggested that early TM compounds such as $TiO_2$, $V_2O_3$, $LaVO_3$, and $Cr_2O_3$ should be placed in the intermediate between CT and the M−H regime with comparable $U$ and $\Delta$. Such changes in the nature of the I-phase arise due to the large value of the p−d$\sigma$ hybridization as a consequence of the extended nature of the early TM 3d orbitals and as a resultant, some of the early transition-metal oxide (TMO) compounds along with $V_2O_3$ are placed in the intermediate insulating regime. Therefore, the large ligand to metal p−d hybridization leads to a strong covalency into the system and can play a crucial role in determining the insulating state of a correlated material. In addition, the electronic correlation can be tailored by tuning various factors such as sample stoichiometry, applying epitaxial strain, chemical doping, external biasing, and so on.[31] Interestingly, Peng et al. demonstrated the conversion of memory switching by tuning the electronic correlation of a strongly correlated NiO system and suggested the profound effect of electronic correlation on the resistive switching mechanism.[31] Therefore, it is important from the technological as well as the fundamental point of view to probe the electronic structure of correlated electron system $V_2O_3$ in the thin film form where the electronic correlation can be tuned using the substrate-induced lattice misfit strain.

In the present study, we have investigated the detailed electronic structure of an epitaxial $V_2O_3$ thin film at both the M-phase (300 K) and the I-phase (120 K) using resonant photoemission spectroscopy (RPES) and X-ray absorption near-edge spectroscopy (XANES). The combined XANES and valence band spectra (VBS) provide an insight into the evolution of electronic correlation strength ($U/W$), which is the driving parameter for the MIT and the origin of the band gap in the strained $V_2O_3$ film. The substrate-induced lattice misfit strain alters the V−O bond topology, which causes an enhancement of the V 3d−O 2p bond covalency in the strained $V_2O_3$ thin film, leading to a CT type ($U > \Delta$) insulating state at low temperature (LT), different from its bulk counterpart.

## RESULTS AND DISCUSSION

**Crystal Structure and Resistivity Measurements.** Figure 1a shows the RT $\theta-2\theta$ XRD patterns of a $V_2O_3$ thin film grown on a (001)-oriented $Al_2O_3$ substrate. The diffraction patterns indicate the single-phase growth of the film with a hexagonal crystal structure oriented along the (001) direction. The out-of-plane lattice parameter of the film is calculated to be 13.96 Å. The in-plane lattice parameter obtained from the RT in-plane $\theta-2\theta$ XRD of the grown film as shown in the inset of Figure 1a is found to be 4.96 A°. The 4% in-plane lattice mismatch between the $V_2O_3$ bulk ($a = b =$ 4.951 A°) and the substrate ($a = b =$ 4.758 A°) would cause an enhancement in the out-of-plane lattice parameter and diminution of the in-plane lattice parameter of the $V_2O_3$ film. However, we observed a reverse scenario for the $V_2O_3$ thin film studied here, where the $V_2O_3$ film exhibits a tensile strain in the in-plane direction, as a resultant of which the lattice parameter along the out-of-plane direction shortens. Such reversal arises due to the huge difference in the thermal expansion coefficient (TEC) between $V_2O_3$ and $Al_2O_3$.[32] Therefore, the lattice mismatch alone cannot explain the above observations; the thermal strain that is generated due to the difference between the TEC should be taken into account in order to understand the alternation of the lattice parameters of the $V_2O_3$ film when deposited over TEC mismatched $Al_2O_3$ substrates.

Figure 1b shows the azimuthal in-plane phi scans of the grown film and the substrate along the (116) reflection. The scans of the $V_2O_3$ thin film and $Al_2O_3$ substrate show six diffraction peaks separated by 60°, which confirm the presence of a sixfold symmetry in the grown film. Moreover, the peak positions of the substrate and the film match together, suggesting the epitaxial growth of the $V_2O_3$ film on the $Al_2O_3$ substrate.

To probe the electrical transport properties of the film, temperature-dependent resistivity measurement of the film was performed, as shown in Figure 1c. The resistivity derivative exhibits a peak at 160 K, designated as transition temperature ($T_c$), which denotes the formation or destruction of percolation conduction.

**Electronic Properties.** *Valence Band Spectroscopy across MIT.* Figure 2 shows the VBS of the epitaxial $V_2O_3$ thin film recorded at an incident photon energy ($h\nu$) of 58 eV

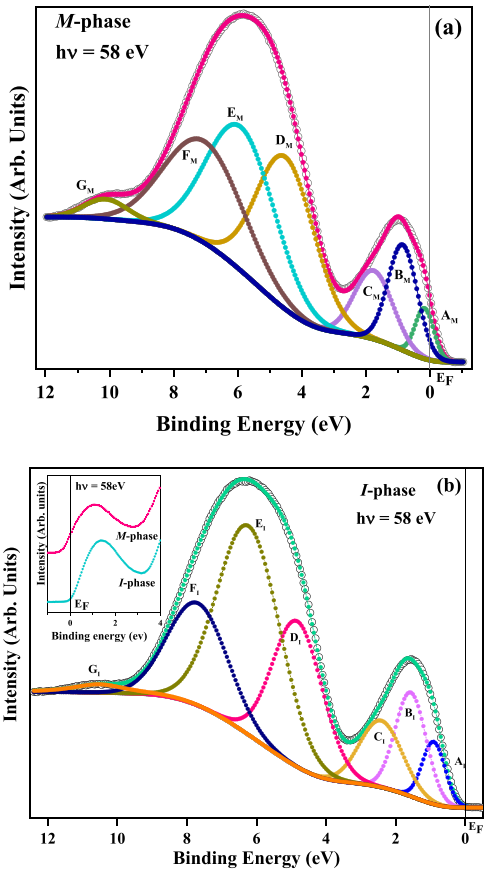


**Figure 2.** VBS analysis of the $V_2O_3$ thin film. (a) Deconvoluted VB photoemission spectrum of the $V_2O_3$ thin film in the M-phase (300 K). (b) Deconvoluted VB photoemission spectrum of the $V_2O_3$ thin film in the I-phase (120 K), both recorded at a 58 eV photon energy with the inset showing a zoomed view near $E_F$ at both 300 and 120 K; the presence of spectral intensity confirming the metallic and absence of spectral intensity confirms the insulating nature of the $V_2O_3$ thin film at 300 and 120 K, respectively.



https://doi.org/10.1021/acsaelm.2c00460
ACS Appl. Electron. Mater. 2022, 4, 3036−3048

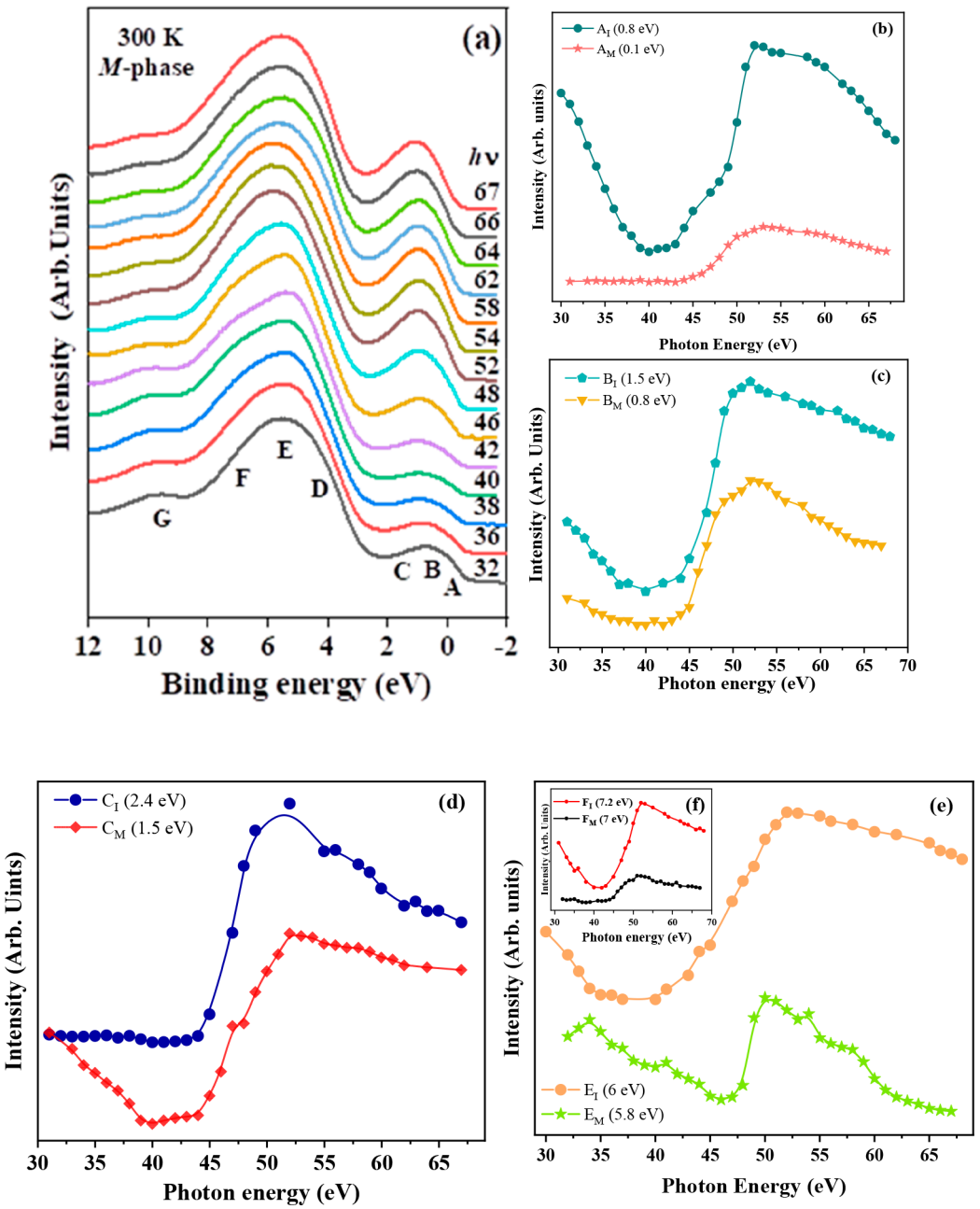


**Figure 3.** Energy-dispersive curves and CIS plots of the $V_2O_3$ film. (a) Energy distribution curves obtained in the M-phase at 300 K for the photon energies between 32 and 68 eV. (b) CIS spectra of features "$A_I$ (0.8 eV)" and "$A_M$ (0.1 eV)" in the VB of the $V_2O_3$ thin film. (c) CIS spectra of features "$B_I$ (1.5 eV)" and "$B_M$ (0.8 eV)" in the VB of the $V_2O_3$ thin film. (d) CIS spectra of features "$C_I$ (2.4 eV)" and "$C_M$ (1.5 eV)" of the $V_2O_3$ thin film. (e) CIS spectra of features "$E_I$ (6 eV)" and "$E_M$ (5.8 eV)" of the $V_2O_3$ thin film: the inset shows the CIS spectra of features "$F_I$ (7.2 eV)" and "$F_M$ (7 eV)".

in the M-phase (300 K) and I-phase (120 K), respectively. The presence of continuous spectral density of states (DOS) at the $E_F$ at RT indicates the metallic nature of the film, whereas the absence of DOS at 120 K is consistent with the insulating nature of the film. We have deconvoluted the VBS with the minimum number of Gaussians and analyzed the different features present in the VBS. The spectrum consists of two main spectral regions: (i) $E_F$ to 3 eV and (ii) 3−9 eV. In the first region, the feature between $E_F$ and 2−3 eV $E_B$ can be referred to as a combination of the Hubbard band (HB) + QP peak.[22,33,34] In the M-phase, such a spectral region is fitted with three peaks centered at around $E_B$ positions 0.1 eV ($A_M$), 0.8 eV ($B_M$), and 1.5 eV ($C_M$). The feature $A_M$ represents the coherent QP feature, where the screening charge comes from the delocalized state at the $E_F$. Features $B_M$ and $C_M$ represent the incoherent features and correspond to the localized electronic states due to electron correlation. The DMFT described the coexistence of coherent QP features close to $E_F$ and an incoherent feature described as a spectral signature of LHB at a higher $E_B$ in the *M*-phase of a correlated $V_2O_3$ compound.[35] The other region between 3 and 9 eV is dominated by O 2p contributions. In agreement with the previous experimental results,[36] the VBS in this $E_B$ range presents a pronounced and broad feature around 6 eV $E_B$, evolving in a clear three-peak structure with a residual tail of intensity at $E_B \geq 10$ eV. The feature $D_M$ around 4.5 eV is


https://doi.org/10.1021/acsaelm.2c00460
ACS Appl. Electron. Mater. 2022, 4, 3036−3048

assigned as O 2p nonbonding orbitals.[36,37] The features $E_M$ and $F_M$ at 5.8 and 7 eV are attributed to the V 3d−O 2p hybridized orbitals, respectively.

In the I-phase of $V_2O_3$ (120 K), besides the absence of spectral DOS at $E_F$, the VBS shift slightly toward a higher $E_B$. We have also fitted the V 3d-dominated region near the $E_F$ with three features, akin to the RT VBS, positioned at 0.8 eV ($A_I$), 1.5 eV ($B_I$), and 2.4 eV ($C_I$) as shown in Figure 2b. The energy positions of the incoherent structures still remain the same as in the M-phase at 0.8 and 1.5 eV. However, it appears that a spectral weight from the coherent states at 0.1 eV in the M-phase shifts to the 2.4 eV $E_B$ position of the I-phase as the system undergoes MIT. An earlier report based on the cluster calculation suggested that in $V_2O_3$, the coherent state present near $E_F$ shifts to a higher $E_B$ (∼3.0 eV) as the M−H screened state with the MIT.[38] The higher $E_B$ region (3−9 eV) is dominated by the O 2p band that is also fitted with three spectral features akin to the VBS of the M-phase as positioned at 4.7 eV ($D_I$), 6 eV ($E_I$), and 7.2 eV ($F_I$). A weak feature "G" is observed at around 10 eV in the M-phase as well as the I-phase, which is attributed to the satellite structure of vanadium.[36,39]

*RPES across MIT.* To understand the origin of different features observed in VBS, we performed the RPES measurements of the $V_2O_3$ film in the metallic as well as insulating regime (at 300 and 120 K, respectively) by recording the VBS at different photon energy values swept through 30−68 eV, which cover the V 3p−3d excitation, as shown in Figure 3a (for the M-phase). It is clearly observed that the intensity of the feature centered at $E_B$ 1 eV increases with the photon energy, and it reaches a maximum at about 52 eV, in both the M- and I-phases. In RPES, such an observed photoemission enhancement is ascribed to the resonant photoemission intensity of the TM-3d derived states.[40,41] It is well known that 3d photoemission is resonantly enhanced at the 3p−3d photoemission due to the occurrence of an indirect process associated with the Super Coster−Kronig decay of the intermediate state reached by photo-absorption, which has the same initial and final states as a direct photoemission process. The direct PE process of a valance V 3d electron is described as

$$\mathrm{V{:}\ 3p^6 3d^2(t_{2g}^2)} + h\nu \rightarrow \mathrm{V{:}\ 3p^6 3d^1(t_{2g}^1)} + \mathrm{e^-}$$

However, the indirect process called Super Coster−Kronig decay occurs as described below

$$\mathrm{V{:}\ 3p^6 3d^2(t_{2g}^2)} + h\nu \rightarrow [\mathrm{3p^5 3d^3}]^* \rightarrow \mathrm{V{:}\ 3p^6 3d^1(t_{2g}^1)} + \mathrm{e^-}$$

The quantum−mechanical interference within the final states of these two processes leads to resonantly enhanced photoemission intensity. However, the atomic O 2p photoionization cross section decreases gradually with the photon energy.[42] Thus, the origin of the resonance at around 52 eV photon energy can be explained on the basis of the quantum-mechanical interference between two excitation processes of the $V^{3+}$ state, consistent with a previous report.[43] The energy of the resonance maximum for $V^{3+}$ in the film is shifted by 10−15 eV from the calculated 3p → 3d threshold energy 37 eV for $V^{3+}$ according to a one-electron picture. In the case of lighter TMOs, this delay in resonance occurs due to the contribution of exchange interaction, which increases the energy of the intermediate excited state $[3p^5 3d^3]^*$.[44]

The variation in the spectral intensity of different features in the VBS with the incident photon energy is revealed more clearly in the constant initial state (CIS) spectra plot, as shown in Figure 3b−e. The CIS spectra are plotted by taking the area under different features for all photon energy values. Figure 3b−e shows the photon energy dependence of the CIS intensity for different features in the metallic as well as the insulating regime. It is observed that the features $A_M$ (0.1 eV), $B_M$ (0.8 eV), and $C_M$ (1.5 eV) for the M-phase and $A_I$ (0.8 eV), $B_I$ (1.5 eV), and $C_I$ (2.4 eV) for the I-phase reveal the resonance enhancement in intensity with the photon energy, indicating the dominant presence of the V 3d band. Interestingly, in the M-phase, the CIS of the feature $A_M$ (0.1 eV) reveals only resonance enhancement, while the CIS of feature $A_I$ (0.8 eV) in the I-phase exhibits an antiresonance dip at around 42 eV photon energy followed by resonance. The CIS of both features $B_M$ (0.8 eV) and $B_I$ (1.5 eV) shows a sharp enhancement along with an antiresonance dip at a lower photon energy. Similarly, the feature $C_M$ (1.5 eV) reveals a resonance followed by an antiresonance dip at 42 eV, while feature $C_I$ (2.4 eV) reveals only a resonance peak without a remarkable antiresonance dip.

It is known that the shape of the resonance profiles obtained from the RPES can be useful to distinguish the nature of the final states associated with the specific feature in VBS.[45] The CIS spectra for the $3d^{n-1}$ final states show only a resonance peak without a remarkable antiresonance dip near the TM 3p→3d threshold, while for $3d^n\underline{L}$ (where $\underline{L}$ denotes a hole in the O 2p band) final states, an antiresonance dip on the lower photon energy side of a shallow peak is accentuated. Thus, the presence of only a resonance peak in the CIS plot for the coherent feature $A_M$ (0.1 eV) in the M-phase suggests the dominant contribution of the $3d^{n-1}$ ($3d^1$) final state character, whereas the incoherent features $B_M$ (0.8 eV) and $C_M$ (1.5 eV) reveal the antiresonance dip followed by the sharp resonance, suggesting its $3d^2\underline{L}$ final state character. In the I-phase, CIS plots of incoherent features $A_I$ (0.8 eV) and $B_I$ (1.5 eV) reveal the antiresonance dip followed by the sharp resonance, suggesting its $3d^2\underline{L}$ nature. The CIS of the unique feature $C_I$ (2.4 eV) in the I-phase of the $V_2O_3$ film shows only resonance enhancement akin to the coherent feature $A_M$ (0.1 eV) of the M-phase, suggesting its dominant contribution of the $3d^{n-1}$ ($3d^1$) final state. Therefore, the similar nature of the final state ($3d^1$) associated with the feature $A_M$ and $C_I$ further confirms that a spectral weight transfer has taken place from the coherent screened state $A_M$ (0.1 eV) to M−H screened states $C_I$ (2.4 eV) as the $V_2O_3$ undergoes MIT. Features $E_M$ (5.8 eV), $F_M$ (7 eV) and $E_I$ (6 eV), $F_I$ (7.2 eV) in the O 2p-dominated region that appeared in both the metallic and the insulating states also show resonance enhancement, which divulges the presence of an appreciable amount of V 3d character. Such resonant enhancement in the O 2p band was also observed in $LaVO_3$ and $YVO_3$[46] and was attributed to O 2p and V 3d hybridization.

*Probing Unoccupied State across MIT.* Figure 4a,b shows the V $L_{3,2}$ and O K-edge X-ray absorption spectroscopy (XAS) spectra of the $V_2O_3$ film, in both the M-phase (300 K) and the I-phase (120 K). The V L-edge spectra correspond to transitions from a well-defined ground state $2p^6 3d^2$ to one of the final states $2p^5 3d^3$ followed by the dipole selection rule. Figure 4a show two broad peaks centered at the position of


https://doi.org/10.1021/acsaelm.2c00460
ACS Appl. Electron. Mater. 2022, 4, 3036−3048

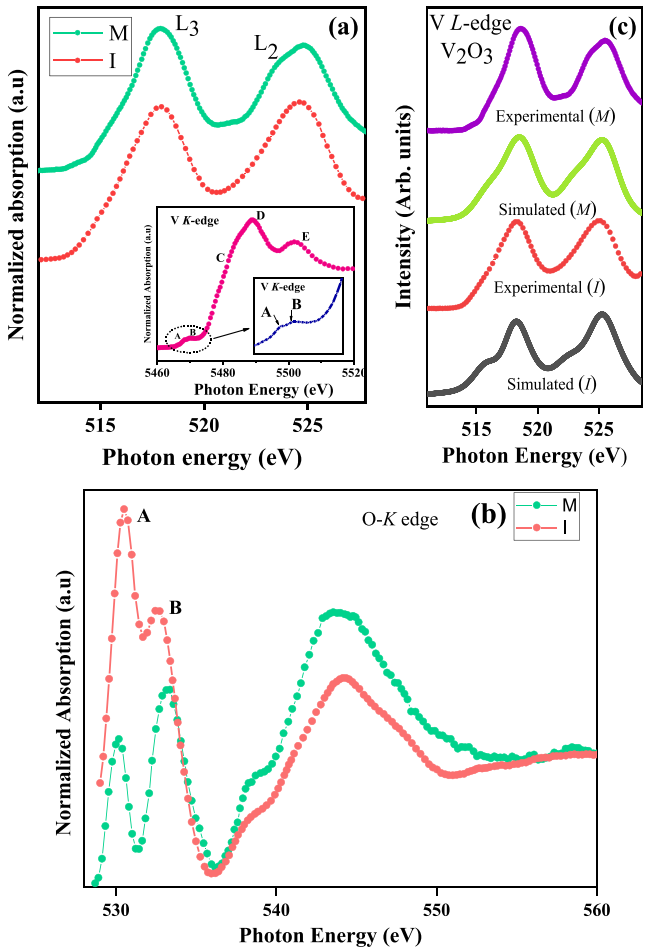


**Figure 4.** XAS analysis of the $V_2O_3$ film across MIT. (a) V L-edge of the $V_2O_3$ thin film in the M-phase (300 K) and I- phase (120 K); the inset shows the V K-edge XANES spectrum of the $V_2O_3$ thin film in the M-phase. (b) O K-edge XANES of the $V_2O_3$ thin film at both the M- and I- phases. (c) Simulated $V^{3+}$ L-edge spectra along with the experimental V L-edge of the $V_2O_3$ thin film at 300 and 120 K.

around 518 and 524.6 eV assigned to $L_3$ (V $2p_{3/2}$−V 3d) and $L_2$ (V $2p_{1/2}$−V 3d) transitions, respectively, owing to the spin−orbit coupling. The overall shape of the spin−orbit split V $L_{3,2}$ absorption peak is determined by the crystal-field effects along with the multiplet effects, which are originated the by 3d−3d Coulomb, the 2p−3d Coulomb, and the exchange interactions.[47] The V $2p_{1/2}$ peak is more broadened than that of V $2p_{3/2}$ due to the Coster−Kronig Auger process.[47,48] These spectra agree well with the previous XAS measurements of the bulk $V_2O_3$,[49] further confirming the $V^{3+}$ state of the grown $V_2O_3$ film. Further, to confirm the oxidation state of V in $V_2O_3$, we have recorded the V K-edge XANES in the M-phase as shown in the inset of Figure 4a. In the distorted octahedral environment of $V_2O_3$, the pre-peak structures A and B appear due to transitions from 1s to 3d−4p hybridized orbitals, whereas feature D is assigned to the dipole-allowed 1s to 4p transition. The pre-peak structures A and B are positioned at photon energies 5468.2 and 5469.6 eV, and feature D is positioned at 5488.9 eV. The photon energy positions of these features and the spectral shape of the V K-edge agree well with the previous reports,[50,51] confirming the $V^{3+}$ state in our grown film.

The O 1s absorption spectrum corresponds to the transitions from the O 1s core level to unoccupied O 2p states hybridized with the V 3d orbitals, as shown in Figure 4b. The features centered at photon energy positions 530.2 and 533.2 eV obtained at the RT O−K edge spectrum correspond to the transitions of the electron from the O 1s core level to hybridized unoccupied O 2p−V 3d $t_{2g}$ ($a_{1g}$ + $e_g^{\pi}$) and V 3d $e_g^{\sigma}$ states, respectively. The presence of intense crystal-field split $t_{2g}$ and $e_g^{\sigma}$ states in the O−K edge spectra of our studied film discards the possibility of other $VO_x$ compositions, clearly confirming the stoichiometric $V_2O_3$ film.[52,53] The feature at a higher photon energy of around 540−545 eV corresponds to the transitions from the O 1s core level to the hybridized O 2p−V 4sp structure. The crystal-field splitting energy calculated from the separation between the $t_{2g}$ and $e_g$ states is found to be 3 eV, which is larger than the value of the bulk (2.1 eV) as well as that of the thin film of $V_2O_3$ (2.46 eV).[47,54] Such an enhanced value of the crystal field in the film studied here can be understood by considering the ligand field theory where the interaction potential ($Q_V$) depends on the metal to ligand distance given by the equation

$$Q_V \approx \frac{q}{4\pi\varepsilon_0 a}\left[6 + \frac{35}{4a^4}\left(x^4 + y^4 + z^4 + \frac{3r^4}{5}\right) + O\left(\frac{r^6}{a^6}\right)\right]$$

where $x$, $y$, $z$, and $r$ are related to the Cartesian co-ordinates and "$a$" is the distance between the center of the octahedron and the charge. It should be noted here that in $V_2O_3$, trigonal distortion further splits the $a_{1g}$ and $e_g^{\pi}$ states, where the splitting depends upon the c/a ratio.[20] Hu et al. have shown that a lower value of $c/a$ offers the larger trigonal distortion in the $V_2O_3$ film, which can also cause an enhancement in the crystal-field splitting energy. Thus, in the $V_2O_3/Al_2O_3$ film studied here, both the substrate-induced lattice misfit strain and the larger trigonal distortion with $c/a$ = 2.81 modify the interaction potential at the center of the octahedron and resultantly, a higher crystal-field value is observed compared to the previous reported $V_2O_3$ bulk and film. Besides, the hybridization strength between V 3d and O 2p is also estimated from the radial extent of the 3d orbital ($r_d$) and the metal−oxygen distance $d_{TM-O}$, using the relationship given by Harrison, $(pd\sigma) \propto r_d^{1.5}/d_{TM-O}^{3.5}$.[55,56] The reduced out-of-plane lattice parameter in the $V_2O_3$ thin film results in a decrease in the V−O bond length, which also leads to the stronger hybridization between V 3d and O 2p orbitals. To get an insight into the changes in the V−O bond lengths of the grown film, we further carried out RT extended X-ray absorption fine structure (EXAFS) measurements as discussed later in the article.

To understand the modification in the unoccupied DOS of $V_2O_3$ upon MIT, we further recorded the O K-edge spectra of the epitaxial $V_2O_3$ film in the I-phase at 120 K. Interestingly, we observed that with the lowering of temperature, the intensity of both features A representing the $t_{2g}$ ($a_{1g}$ + $e_g^{\pi}$) band and feature B ($e_g^{\sigma}$ band) sharply increases in the I-phase compared to the M-phase. Moreover, in the I-phase, the intensity of the $t_{2g}$ feature is enhanced in comparison to that of $e_g^{\sigma}$. It is important to note that the charge state or the valance state of vanadium remains unchanged ($V^{3+}$) across MIT in $V_2O_3$ as confirmed from the same onset position of the V L edge XAS at both the temperatures and LT XPS (not shown here). Hence, the enhancement in the intensity of the unoccupied V $t_{2g}$ and $e_g$ bands may be due to the modifications


https://doi.org/10.1021/acsaelm.2c00460
ACS Appl. Electron. Mater. 2022, 4, 3036−3048

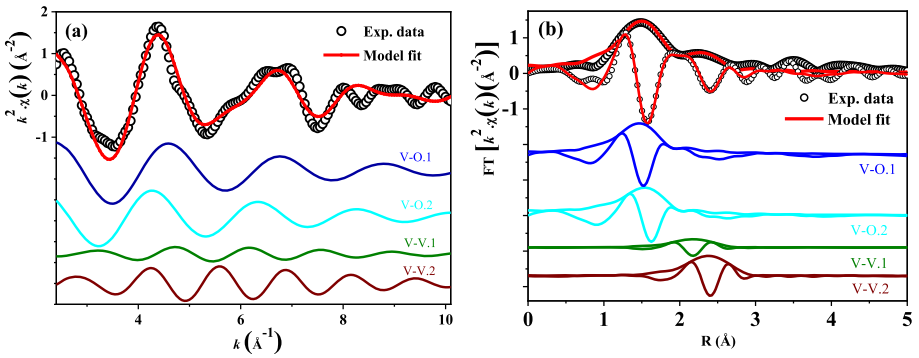


**Figure 5.** EXAFS study of the $V_2O_3$ film. V K-edge EXAFS analysis; (a) $k^2$-weighted spectra and (b) modulus, the imaginary part of the Fourier transforms presents the observed signals (hollow/black circles) and their best fits (solid/red lines) for the $V_2O_3$ thin film. Contributions from different coordination shells in the EXAFS spectra are presented with arbitrary vertical shifts.

in hybridization between V 3d ($t_{2g}$) and O 2p in the I-phase. The MIT in $V_2O_3$ is associated with a structural transition from the RT corundum to the LT monoclinic phase. In the LT monoclinic phase, an expansion in the V−V bond length and rotation of V−V bond direction of about 1.8° from the *c*-axis, that is, with respect to the basal plane results in squeezing of the oxygen octahedral.[22] Such squeezing of octahedra results in increasing the hybridization between the V $a_{1g}$ orbitals (orbitals directed toward the basal plane) and O 2p orbitals, which can result in an enhancement of feature A at 120 K. Besides such enhancement, the energy positions of the first feature in O K-edge absorption spectra obtained at the I-phase slightly shifts toward a higher photon energy as compared to the metallic state. Such shifting in the position toward a higher photon energy can be attributed to an increase in $U/t$ as a consequence of decrease in dielectric screening.[56,57] The crystal-field splitting energy in the I-phase is calculated to be 2.2 eV from the experimental XAS spectra.

*CT Multiplet Calculation.* To better understand the V L edge of the strained $V_2O_3$ film in the metallic and I-phases, we have simulated the $V^{3+}$ L-edge spectrum by the CT multiplet program for XAS (CTM4XAS) under the ligand field and CT multiplet approach.[58] The CT multiplet calculations are performed by varying the reduction in Slater integrals, crystal-field splitting 10Dq, CT parameters like CT energy Δ, d−d interaction energy $U_{dd}$, the core hole potential $U_{pd}$ ($U_{pd} \approx 1.25U_{dd}$), and p−d transfer integral T for both the M- and I-phases of the $V_2O_3$ film. Figure 4c shows the simulated $L_{2,3}$ spectrum of $V^{3+}$ along with the experimental V L-edge of a strained $V_2O_3$ film at 300 and 120 K, respectively. The Lorentzian of 0.4 eV and Gaussian of 0.3 eV are used for convolution of the simulated spectrum. To compare the experimental spectra, broadening due to the presence of several intrinsic broadening mechanisms such as lifetime effects, vibrations, hybridization (covalency), and so on are also taken into consideration. It is important to highlight that in oxides, the covalency introduces more broadening in the experimental spectra.[47] For the simulation, the symmetries are limited to octahedral ($O_h$), tetragonal ($D_{4h}$), and fourfold symmetry ($C_4$). The distortion from a perfect $O_h$ symmetry to a $D_{4h}$ symmetry causes the splitting of $t_{2g}$ orbitals into lower-lying $e_g^{\pi}$ and upper lying $a_{1g}$ orbitals in $V_2O_3$. In the $D_{4h}$ geometrical symmetry, *T* ($b_1$), *T* ($a_1$), *T* ($b_2$), *T* (e) symmetries are related to $x^2 - y^2$, $z^2$, *xy*, and *xz*/*yz* orbitals, respectively. In the M-phase, the Slater integrals are reduced to 60% of the Hartree−Fock values, and the parameters used for simulation are as follows: d−d interaction energy ($U_{dd}$) = 1 eV, core-hole potential ($U_{pd}$) = 2 eV, CT energy (Δ) = 1.8 eV, crystal-field splitting (10D*q*) = 3 eV, and hopping parameter T ($b_1$) = 3.6 eV. In early TM compounds, due to the extended nature of 3d electrons, the hybridization results in a reduction of mutual interactions. Hence, it is important to highlight that this hybridization effect can be simulated by an extra reduction of the two-particle interaction parameters $F_{dd}^2$ and $F_{dd}^4$.[47] Hence, the reduction of Slater integrals to 60% of the Hartree-Fock values as compared to the reported 80% in the bulk $V_2O_3$[30] suggests the increase in covalency in our grown film in comparison to the bulk $V_2O_3$. Similarly, we have fitted the RT core level V 2p XPS spectrum of the $V_2O_3/Al_2O_3$ film studied here using the CTM4XAS software (not shown here). The obtained simulated XPS spectrum appears to be well matched with the experimental result, which further confirms the reliability of our experimentally extracted electronic parameters from the combined VBS and XAS spectra. In the simulated XPS spectrum, we have used slightly higher Lorentzian and Gaussian broadening of 0.6 and 1 eV as compared to simulated XAS owing to the different core-hole final state and instrumental broadening. In the I-phase, the Slater integrals were also reduced as compared to the bulk value. The parameters used for simulation are d−d interaction energy ($U_{dd}$) = 4.2 eV, core-hole potential ($U_{pd}$) = 5.5 eV, CT energy (Δ) = 2.6 eV, crystal-field splitting (10D*q*) = 2.2 eV, and hopping parameter *T* ($b_1$) = 3 eV.

*Local Structure Using EXAFS.* As the EXAFS is a very useful technique to realize the local geometric structure around the absorption site, we have performed the V K-edge EXAFS measurement of a strained $V_2O_3$ thin film at RT. Figure 5a,b shows a $k^2$-weighted signal in *k*-space and corresponding modulus, imaginary part of Fourier transforms (FT), respectively, of V K-edge EXAFS spectra for a strained $V_2O_3$ thin film. For modeling of the experimental data, we have used the $R\bar{3}C$ space group (corundum structure), and the atomic positions used are taken from the previous literature on bulk.[59] The fits were confined to an *R*-range of 1 Å ≤ *R* ≤ 3 Å and a *k*-range of 2.5 $Å^{-1} \leq k \leq 10$ $Å^{-1}$. Within this fitted region, EXAFS spectra originate because of photoelectron scattering from the first nearest neighbor octahedral O atoms and the second nearest neighbor V atoms. During refinement, the same amplitude reduction factor ($S_0^2$) and energy shift ($\Delta E_0$) were used for all coordination shells. In the EXAFS theoretical model, for each coordination shell, atomic pair separations (*R*) and mean-square relative displacement factors ($\sigma^2$) were


https://doi.org/10.1021/acsaelm.2c00460
ACS Appl. Electron. Mater. 2022, 4, 3036−3048

refined to adequately reproduce the experimentally observed pattern. Some preliminary fitting trials show that both $R$ and $\sigma^2$ for V−O (1) and V−O (2) scattering paths are highly correlated. Therefore, the same $R$ and $\sigma^2$ parameters are used for V−O (1) and V−O (2) scattering paths. A similar constraint is also considered for the $\sigma^2$ value of V− V (1) and V−V (2) coordination shells. The best fit of EXAFS spectra in $k$-space and $R$-space as shown in Figure 5a,b indicates a reasonable agreement between the theoretical model and experimental pattern. Obtained values of structural parameters are listed in Table 1. EXAFS analysis reveals that in the studied

**Table 1. Structural Parameters for a Strained $V_2O_3$ Thin Film and $V_2O_3$ Bulk from ref 59[a]**

| $V_2O_3/Al_2O_3$ (001) thin film | | | $V_2O_3$ bulk[59] |
|---|---|---|---|
| bond | $\sigma^2$ ($10^{-3}$ Å$^2$) | $R$ (Å) | $R_{eff}$ (Å) |
| V−O (1) | 7 (1) | 1.938 (2) | 1.96300 |
| V−O (2) | 7 (1) | 2.036 (2) | 2.06190 |
| V−V (1) | 10 (2) | 2.656 (9) | 2.69680 |
| V−V (2) | 10 (2) | 2.875 (9) | 2.88200 |

[a]Numbers in parentheses represent the error bar on the last digit.

$V_2O_3$ thin film, V−O as well as V−V coordination distances reduce as compared to the $V_2O_3$ bulk.[59] A previous XRD refinement study on doped (Cr and Ti) single crystal $V_2O_3$ revealed enhanced V (1)−V (2) and V (1)−O (1) bond distances.[60] However, the nature and effective length scale of the strain in the chemically doped system could be different from the epitaxial strain in the film.[61] It is quite evident that effectively the $VO_6$ octahedron shrinks as all the V−O bond distances have shortened with respect to the corresponding bulk values. This shrinkage leads to enhancement in the hybridization strength and crystal-field splitting for the $V_2O_3$ thin film studied here, as observed in the XAS analysis.

*Electronic Structure near the Vicinity of Fermi Energy ($E_F$) across MIT.* The experimental VBS and conduction band (CB)(oxygen K-edge) spectra of an epitaxial $V_2O_3$ film are combined to study the modifications in the band structure around the $E_F$ as the temperature is varied across MIT, as shown in Figure 6. We have used the O K-edge spectrum for the representation of the CB because the core-hole effect on the final state density of state in the O K-edge is considerably lesser compared to that of TM 2p edges.[40] The $E_F$ is determined with respect to the O K-edge XAS spectrum by subtracting the photon energy position of the O K-edge spectrum from the O 1s core level $E_B$ position of the $V_2O_3$ film obtained from XPS. In the M-phase, two prominent features are observed in the CB of the O−K edge at 0.8, 3.8 eV and one broad feature at around 15 eV. The feature centered at around 0.8 eV arises primarily from the unoccupied part of the crystal-field split $t_{2g}$ ($a_{1g}$ + $e_g^{\pi}$) band and represents the spectroscopic signature of the UHB. The completely empty $e_g^{\sigma}$ band appears at a higher energy of 3.8 eV. The last feature (at 15 eV) is attributed to the V 4s−4p band hybridized with O 2p. From the RT VBS, it is realized that the coherent band near $E_F$ (at 0.1 eV) is dominated by the V 3d character and represents the LHB. The value of on-site Coulomb repulsion energy "$U$" is the energy difference between the LHB and UHB, and the CT energy "Δ" is the energy difference between the O 2p band and UHB. From the combined spectra in the M phase, $U$ is estimated to be 1 eV and Δ is estimated to be 1.8 eV. The combined spectra in the $I$-phase reveal $U$ and Δ as 4.2 and 2.6

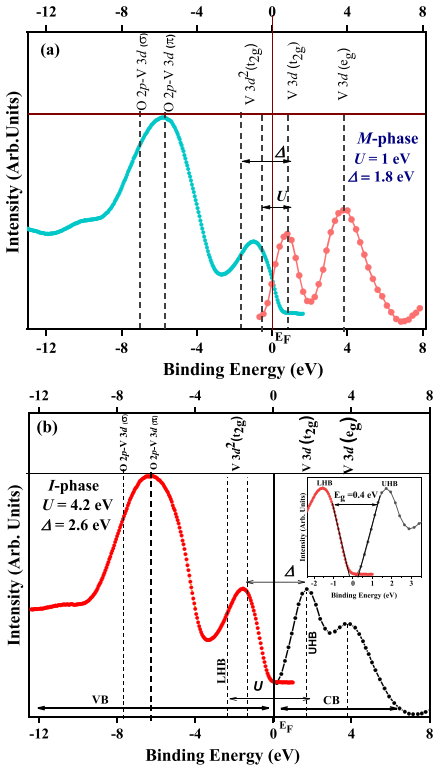


**Figure 6.** Band structure near the $E_F$, derived from the combined experimental VB and CB of the $V_2O_3$ film across MIT. (a) Band diagram near the $E_F$, derived from the experimental VB and CB of the $V_2O_3$ thin film in the M-phase (300 K). (b) Band diagram near the $E_F$, derived from the experimental VB and CB of the $V_2O_3$ thin film in the I- phase (120 K).

eV, respectively. These values are similar to those obtained from the simulation of the V L edge from the CT multiplet program. The obtained higher value of Δ compared to the $U$ ($U$ > Δ) clearly demonstrates the low-temperature CT-type insulating nature of the studied strained epitaxial $V_2O_3$ film.

The Hubbard model explained well the kinetics of correlated systems in terms of the kinetic or hopping term $t$ and on-site Coulomb repulsion $U$.[3] The kinetic part favors the itinerant behavior of electrons, while the Coulomb repulsion tries to localized electrons at their respective atomic sites, and hence, a delicate balance between $U$ and $W$ (=2$Zt$, $Z$: number of nearest neighbors) governs the MIT in correlate electronic systems. The electronic correlation strength parameter defined as the ratio of the Coulomb interaction $U$ and the bandwidth $W$ ($U$/$W$) determines the electronic properties of correlated systems as described by the Hubbard model.[1,11] From the combined spectra of $V_2O_3$ in the M-phase (shown in Figure 6a), the electronic correlation strength is calculated to be $U/W$ = 0.4 and the CT energy is calculated to be 1.8 eV. At RT, the presence of a QP peak (at 0.1 eV) near $E_F$ and $U/W$ = 0.4 reveals the strongly correlated metallic nature of the $V_2O_3$ film. The obtained electronic correlation strength $U/W$ is larger as compared to previous studies.[62] The origin of such disparity lies in the different ways of $U/W$ estimation. In previous studies, $W$ is estimated from band structure calculations,[62,63] and it is shown that the obtained theoretical value of $W$ is nearly double the value obtained from the photoemission spectroscopic experiment.[64] Besides, there is also inconsistency in the measured value of Coulomb correlation energy ($U$) using high-energy spectroscopy and low-energy optical


https://doi.org/10.1021/acsaelm.2c00460
ACS Appl. Electron. Mater. 2022, 4, 3036−3048

conductivity techniques. For example, in XAS, sometimes the transition to the lower empty sate is forbidden by the selection rule (dipole transition), which inevitably shifts the XAS edge and hence increases the $U$. Moreover, $U$ is higher in the thin film compared to its bulk counterpart as the two-dimensionality enhances the $U$ due to the reduced dielectric screening. These effects altogether could effectively enhance the $U/W$ value. The Mott MIT occurs when the electron interactions are sufficiently strong to cause the QP peak to vanish as the spectral weight of that low-frequency peak is transferred to the high-frequency Hubbard bands with opening a band gap. This is quite evident from the CB and valence band (VB) combined spectra of the $V_2O_3$ film in the insulating state, which clearly reveal the opening of the gap, calculated to be 0.4 eV, and the enhanced electronic correlation strength calculated to be $U/W$ = 1.8.

## DISCUSSIONS

According to the phenomenological model proposed by the Zaanen−Sawatzky−Allen,[29] $V_2O_3$ is suggested to be a d band-correlated metal at RT and an M−H type of insulator with a d−d type of lowest energy charge fluctuation in the I-phase. However, some previous studies based on experiments and theory suggested a few early TM compounds along with bulk $V_2O_3$ to be placed intermediate between M−H and CT regimes owing to the equivalent value of $U\sim\Delta$.[30] In the present study of an epitaxial $V_2O_3$ film, the CIS spectra of a coherent feature in the M-phase reveal the dominated V 3d character with a $3d^{n-1}$ final state configuration. Hence, the lowest energy charge fluctuation across the $E_F$ in the M-phase of the $V_2O_3$ thin film is of a $3d^1$ to $3d^3$ type (d−d type). However, the CIS spectra of incoherent features $A_I$ (0.8 eV) and $B_I$ (1.5 eV) near $E_F$ in the I-phase divulge the $3d^2\underline{L}$ final state configuration akin to the M-phase. Due to the transfer of spectral DOS from near the $E_F$ coherent state to the higher $E_B$ M−H screened state across MIT, the I-phase of the epitaxial $V_2O_3$ thin film is governed by the lowest charge fluctuation of the type of $3d^2\underline{L}$ to $3d^3$ configuration. The $3d^2\underline{L}$ final state of the incoherent feature confirms the strong screening from the O 2p states and suggests the dominant presence of O 2p orbitals in the form of hybridization with V 3d orbitals, which makes the lowest energy charge fluctuation of a p−d type in the insulating state of $V_2O_3$. The obtained $U > \Delta$ from the combined spectra and the p−d type of lowest energy charge fluctuation unequivocally confirms the LT CT-type insulating state of the strained epitaxial $V_2O_3$ film. This realization of the insulating state in the epitaxial $V_2O_3$ thin film is different from that of its bulk $V_2O_3$ counterpart. The emergence of the band gap is realized due to the transfer of spectral weight from coherent band $A_M$ in the M-phase to the M−H screened state in the I-phase at around 2.4 eV. Our observations are in accordance with the earlier cluster model calculations on $V_2O_3$, which concluded that the coherent QP feature $3d^2\underline{C}$ (where $\underline{C}$ denotes a hole in the coherent band) has a dominant V 3d character, whereas the incoherent feature has a mainly $3d^2\underline{L}$ nature and possesses a mixed V 3d−O 2p character.[38] The band structure of the $V_2O_3$ thin film at both the M-phase (300 K) and the I-phase (120 K) can be clearly understood from the schematic band diagram (shown in Figure 7), which clearly divulges that the electronic correlation strength ($U/W$) increases as the system undergoes MIT. In a previous study, Fujiwara et al. reported that the $U$ values did not change through the MIT by probing the $E_B$ position of LHB using high-resolution hard XPS.[65] However, in the present study, our RPES analysis performed in the photon energy range of 30−68 eV reveals a clear transfer in the V 3d state position toward the higher $E_B$ side under MIT. It should be noted that this photon energy range offers a relatively higher V 3d/O 2p photoionization cross section, which allows us to probe minute changes in the spectral intensity of VBS.

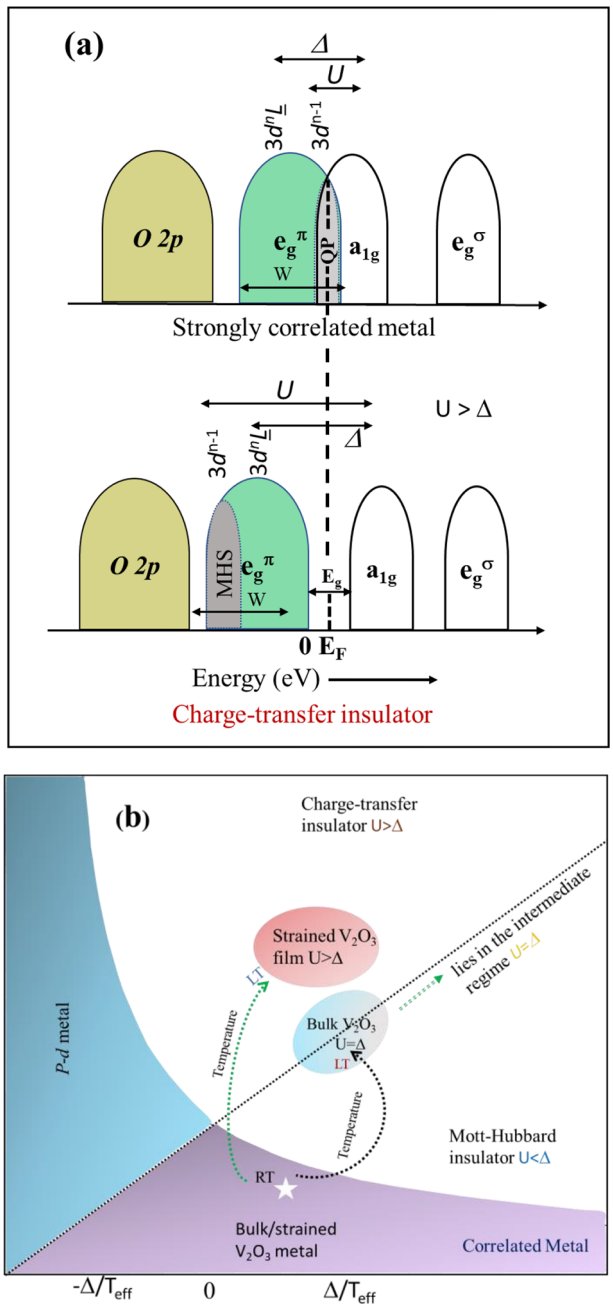


**Figure 7.** (a) Schematic illustration of a strongly correlated metallic nature and CT-type insulating nature of an epitaxial $V_2O_3$ thin film. (b) $\Delta-U$ plot for the grown $V_2O_3$ film lying in the CT regime with a previously reported $V_2O_3$ bulk sample placed in the intermediate regime. The region above the line ($U = \Delta$) is the CT regime, while below it is the Mott−Hubbard regime.

It is important to mention here that the substrate-induced strain plays a vital role in modifying electronic properties in the thin-film form compared to bulk $V_2O_3$. The lower value of c/a modifies the local electronic structure by reducing the V−O



https://doi.org/10.1021/acsaelm.2c00460
ACS Appl. Electron. Mater. 2022, 4, 3036−3048

bond lengths of the $V_2O_3$ thin film studied here as observed from the EXAFS study. Such a reduction in the V−O bond lengths results in an enhanced crystal-field splitting as well as V 3d−O 2p pd$\sigma$ hybridization. As a result, the strained epitaxial $V_2O_3$ thin film shows the CT (p−d) type of insulating character in the insulating regime in contrast to the intermediate of the CT and M−H insulating character of its bulk counterpart, shown schematically in Figure 7b. Shortening of both V−V and V−O bond lengths appears to be different from observations made from the XRD pattern, which revealed the elongation in in-plane and shortening along out-of-plane lattice parameters with respect to bulk $V_2O_3$. Here, we want to highlight that in the case of the $V_2O_3$ thin film studied by us, the EXAFS model fits were confined to the $R$-range of 1 Å $\leq R \leq$ 3 Å, which mainly covers the single $VO_6$ octahedra along with second co-ordination of the V−V linkage. Here, we have not calculated the parameters of the entire unit cell but the first and second nearest neighbor distances only. Using EXAFS data, we probed the modification in the $VO_6$ octahedra of the unit cell since the transport or electronic properties are primarily governed by the nature of the $VO_6$ octahedra. Further, we would like to mention here that in distorted octahedral systems such as $V_2O_3$, the local structural parameters determined from the EXAFS study may deviate from the average structural parameters determined using diffraction measurements.[66] Recently, Chowdhury et al. extensively studied the electronic and magnetic properties of $SrCoO_{2.5}$ thin films via strain engineering and discussed its huge technological applications by modifying the electronic correlations.[40] Tuning the resistance states, especially the nonvolatile resistive switching via strain in heterostructures such as $V_2O_3$/PMN-PT and $VO_2$/PMN-PT, is an active field and provides a potential strategy for designing prototype devices in the information storage industry.[26,67] In the present study, the different competing electronic correlation energetics responsible for the CT type insulating character of the $V_2O_3$ thin film in contrast to its bulk via strain engineering may lead to a unique switching mechanism where besides electrons in metal 3d band, holes in the ligand 2p band can participate in low-energy-charge fluctuation, which may lead to a next-generation efficient resistive switching device.

## CONCLUSIONS

We have studied the modifications in the electronic structure across MIT of an epitaxial $V_2O_3$ thin film grown on a single-crystalline $Al_2O_3$ (001) substrate by pulsed laser deposition (PLD). Lattice mismatch results in the in-plane tensile and out-of-plane compressive strain in the grown film. In temperature-dependent VBS, a spectral weight transfer is clearly observed from the metallic coherent band ($A_M$) to the insulating M−H screened band ($C_I$) across MIT, resulting in an opening of a band gap. A substrate-induced lattice misfit strain reduces the V−O as well as V−V coordination distances compared to the $V_2O_3$ bulk. The effective shrinkage of the $VO_6$ octahedra and reduction in V−O bond distances in the $V_2O_3$ film causes an enhancement in the crystal-field energy and O 2p and V 3d hybridization strength compared to those of the bulk counterpart. The combined CB spectra and VBS in the insulating state suggest the CT type ($U > \Delta$) of the insulating nature of the $V_2O_3$ thin film at LT. The enhanced covalency arises due to the combined effect of the lattice parameter and TEC mismatch between $V_2O_3$ and the $Al_2O_3$ substrate, resulting in the stronger hybridization between O 2p and V 3d in the $V_2O_3$ film studied here, which leads to the decrease in the CT energy compared to that of the bulk $V_2O_3$ in the insulating regime. Our results provide a better understanding of different competing electronic energetics that can be tailored using epitaxial strain and offers an alternate approach to new-generation correlation-derived switching devices.

**Methods.** *Sample Growth.* A single-phase $V_2O_3$ thin film was grown on the (001)-oriented single-crystalline $Al_2O_3$ substrate using PLD techniques. For the thin-film growth, a dense pallet of a single-phase $V_2O_5$ bulk target was used. During deposition of the $V_2O_3$ film, the substrate to target distance was kept at 4.5 cm, the laser energy density at 1.6 J/cm$^2$, and the laser repetition rate at 5 Hz. The base pressure inside the chamber during deposition was maintained at $3 \times 10^{-6}$ mBar and the substrate temperature ($T_s$) was maintained at 650 °C. After deposition, the film was cooled to RT at a rate of 10 °C/min in the same base pressure as used during deposition. The thickness of the film was calculated to be 35 nm using X-ray reflectivity (not shown here).

*Structural Characterization.* The structural characterization was performed using a Bruker D2 Phaser X-ray diffractometer with Cu K$\alpha$ ($\lambda$ = 1.5406 Å) radiation. The in-plane $\theta-2\theta$ XRD and phi scan were done using a Bruker D8-Discover high-resolution X-ray diffractometer. The resistance versus temperature measurement (300−5 K) was carried out using a homemade resistivity set-up in a four-probe configuration.

*VBS and RPES.* The core-level photoelectron spectra of the film were recorded using an Al K$\alpha$ (1486.6 eV) X-ray source and the Omicron energy analyzer (EA-125, Germany). VB measurements were performed at different photon energy values in the range of 30−68 eV in both the M-phase (300 K) and the I-phase (120 K) at the angle-integrated photoemission spectroscopy beamline using an Indus-1 synchrotron source at RRCAT, Indore, India. Prior to the photoemission measurements, the grown film was cleaned using in situ low-energy $Ar^+$ ions. During the spectroscopy measurements, the base pressure of the experimental chamber was maintained in the order of $10^{-10}$ Torr. For calibration of binding energies, the Au foil was kept in electrical contact with the sample, and $E_F$ was aligned using the VBS of the Au foil. During the VBS measurements, the pass energy was kept at 20 eV. The experimental resolution was estimated to be 0.3 eV for the VBS. The background of the core level and VBS were corrected using the Shirley method.

*Extended X-ray Absorption Fine Structure.* Local structural configurations of the $V_2O_3$ thin film were probed using EXAFS measurements at BL-9, Indus-2 synchrotron source, RRCAT, Indore, India. RT V K-edge EXAFS spectra were recorded in fluorescence yield mode, and the estimated energy resolution ($\Delta E/E$) across the measured energy range is about $10^{-4}$. The absorption edge of the V metal foil was used for energy calibration. After standard background subtraction and normalization, EXAFS spectra were fitted with a specific model implementing ARTIEMIS software that uses ATOMS and FEFF6[68] programs to simulate the theoretical spectrum by summing up all partial contributions from scattering paths for a given crystallographic structure.

*X-ray Absorption Spectroscopy.* To probe the unoccupied states of the $V_2O_3$ film, XANES was carried out in the M-phase (300 K) and the I-phase (120 K) using soft X-ray absorption spectroscopy with an experimental resolution of 0.25 eV in the total electron yield mode at beamline BL-01, Indus −2 synchrotron source at RRCAT, Indore, India.



https://doi.org/10.1021/acsaelm.2c00460
ACS Appl. Electron. Mater. 2022, 4, 3036−3048

## AUTHOR INFORMATION


### Corresponding Author

**Ram Janay Choudhary** − *UGC DAE Consortium for Scientific Research, Indore 452001 Madhya Pradesh, India;* orcid.org/0000-0003-0029-1541; Email: ram@csr.res.in

### Authors

**Sophia Sahoo** − *UGC DAE Consortium for Scientific Research, Indore 452001 Madhya Pradesh, India*

**Anupam Jana** − *UGC DAE Consortium for Scientific Research, Indore 452001 Madhya Pradesh, India;* orcid.org/0000-0002-2967-9315

**Anita Bagri** − *UGC DAE Consortium for Scientific Research, Indore 452001 Madhya Pradesh, India*

**Supriyo Majumder** − *UGC DAE Consortium for Scientific Research, Indore 452001 Madhya Pradesh, India*

**Parasmani Rajput** − *Beamline Development and Application Section, Bhabha Atomic Research Center, Mumbai 400085, India*

**Shambhu Nath Jha** − *Beamline Development and Application Section, Bhabha Atomic Research Center, Mumbai 400085, India*

**Frank M. F. de Groot** − *Inorganic Chemistry and Catalysis, Debye Institute for Nanomaterials Science, Utrecht University, 3584 CG Utrecht, The Netherlands;* orcid.org/0000-0002-1340-2186

**Deodatta Moreshwar Phase** − *UGC DAE Consortium for Scientific Research, Indore 452001 Madhya Pradesh, India*

Complete contact information is available at: https://pubs.acs.org/10.1021/acsaelm.2c00460


### Author Contributions

S.S. and R.J.C. contrived the concept. S.S. performed the thin-film deposition with assistance from R.J.C. and acquired the XRD and R versus T data. S.S., A.J., and A.B. obtained and analyzed the XAS and RPES data with assistance from D.M.P. and R.J.C. EXAFS data were collected with help from P.R. and S.N.J. S.S. and S.M. analyzed the EXAFS data. S.S. analyzed and discussed the RPES and XAS studies with R.J.C., A.J., and F.M.F.d.G., with valuable feedback from D.M.P.

### Notes

The authors declare no competing financial interest.

## ACKNOWLEDGMENTS

The authors would like to thank Dr. V. R. Reddy for the phi scan measurement. They are also thankful to Dr. Rajiv Rawat for resistivity measurement. They also acknowledge A. Wadikar, Sharad Karwal, and Rakesh Sah for their technical assistance in RPES and XANES measurements.

## REFERENCES


(1) Imada, M.; Fujimori, A.; Tokura, Y. Metal-insulator Transitions. *Rev. Mod. Phys.* **1998**, *70*, 1039.

(2) Yanase, Y.; Jujo, T.; Nomura, T.; Ikeda, H.; Hotta, T.; Yamada, K. Theory of superconductivity in Strongly Correlated Electron Systems. *Phys. Rep.* **2003**, *387*, 1−149.

(3) Khomskii, D. I. *Transition Metal Compounds*; University of Koln, 2014.

(4) Rao, C. N. R.; Raveau, B. *Transition Metal Oxides*, 2nd ed.; Wiley: New York, 1998.

(5) Jiang, L.; Qu, Y.; Ren, Z.; Yu, P.; Zhao, D.; Zhou, W.; Wang, L.; Fu, H. In Situ Carbon-Coated Yolk−Shell $V_2O_3$ Microspheres for Lithium-Ion Batteries. *ACS Appl. Mater. Interfaces* **2015**, *7*, 1595−1601.

(6) Wang, H.-E.; Zhao, X.; Yin, K.; Li, Y.; Chen, L.; Yang, X.; Zhang, W.; Su, B.-L.; Cao, G. Superior Pseudocapacitive Lithium-Ion Storage in Porous Vanadium Oxides@C Heterostructure Composite. *ACS Appl. Mater. Interfaces* **2017**, *9*, 43665−43673.

(7) Yu, Y.; Huang, S.; Wang, B.; Tie, D.; Wang, Q.; Hou, Y.; Zhao, Y. Achieving High-Energy Full-Cell Lithium-Storage Performance by Coupling High-Capacity $V_2O_3$ with Low-Potential Ni2P Anode. *ACS Appl. Mater. Interfaces* **2019**, *11*, 19−25.

(8) Hassan, N.; Riaz, J.; Qureshi, M. T.; Razaq, A.; Rahim, M.; Toufiq, A. M.; Shakoor, A. Vanadium oxide (V2O3) for Energy Storage applications through Hydrothermal Route. *J. Mater. Sci. Mater. Electron.* **2018**, *29*, 16021−16026.

(9) Lee, M.-H.; Kalcheim, Y.; Valle, J. D.; Schuller, I. K. Controlling Metal−Insulator Transitions in Vanadium Oxide Thin Films by Modifying Oxygen Stoichiometry. *ACS Appl. Mater. Interfaces* **2021**, *13*, 887−896.

(10) Pergament, A.; Stefanovich, G. Insulator-to-Metal Transition in Vanadium Sesquioxide: does the Mott Criterion Work in this case. *Phase Transitions* **2012**, *85*, 185−194.

(11) Panaccione, G.; Altarelli, M.; Fondacaro, A.; Georges, A.; Huotari, S.; Lacovig, P.; Lichtenstein, A.; Metcalf, P.; Monaco, G.; Offi, F.; Paolasini, L.; Poteryaev, A.; Tjernberg, O.; Sacchi, M. Coherent Peaks and Minimal Probing Depth in Photoemission Spectroscopy of Mott-Hubbard Systems. *Phys. Rev. Lett.* **2006**, *97*, 116401.

(12) Hansmann, P.; Haverkort, M. W.; Toschi, A.; Sangiovanni, G.; Rodolakis, F.; Rueff, J. P.; Marsi, M.; Held, K. Atomic and Itinerant Effects at the Transition-Metal X-ray absorption K Pre-edge Exemplified in the case of $V_2O_3$. *Phys. Rev. B: Condens. Matter Mater. Phys.* **2012**, *85*, 115136.

(13) Thomas, G. A.; Rapkine, D. H.; Carter, S. A.; Millis, A. J.; Rosenbaum, T. F.; Metcalf, P.; Honig, J. M. Observation of the Gap and Kinetic Energy in a Correlated Insulator. *Phys. Rev. Lett.* **1994**, *73*, 1529.

(14) Grygiel, C.; Simon, C.; Mercey, B.; Prellier, W.; Limelette, P.; Fresard, R. Thickness Dependence of the Electronic Properties in V2O3 thin films. *Appl. Phys. Lett.* **2017**, *91*, 262103.

(15) Sakai, J.; Limelette, P.; Funakubo, H. Transport Properties and c/a ratio of $V_2O_3$ Thin films Grown on C- and R-plane Sapphire Substrates by Pulsed Laser Deposition. *Appl. Phys. Lett.* **2015**, *107*, 241901.

(16) McWhan, D. B.; Rice, T. M.; Remeika, J. P. Mott Transition in Cr-Doped $V_2O_3$. *Phys. Rev. Lett.* **1969**, *23*, 24.

(17) Lo Vecchio, I.; Baldassarre, L.; D'Apuzzo, F.; Limaj, O.; Nicoletti, D.; Perucchi, A.; Fan, L.; Metcalf, P.; Marsi, M.; Lupi, S. Optical Properties of $V_2O_3$ in its whole Phase Diagram. *Phys. Rev. B: Condens. Matter Mater. Phys.* **2015**, *91*, 155133.

(18) Mansart, B.; Barinov, A.; Dudin, P.; Baldassarre, L.; Perucchi, A.; Papalazarou, E.; Metcalf, P.; Lupi, S.; Marsi, M. Photoemission Microscopy Study of the two Metal-Insulator Transitions in Cr-Doped $V_2O_3$. *Appl. Phys. Lett.* **2012**, *100*, 014108.

(19) Lupi, S.; Baldassarre, L.; Mansart, B.; Perucchi, A.; Barinov, A.; Dudin, P.; Papalazarou, E.; Rodolakis, F.; Rueff, J.-P.; Itié, J.-P.; Ravy, S.; Nicoletti, D.; Postorino, P.; Hansmann, P.; Parragh, N.; Toschi, A.; Saha-Dasgupta, T.; Andersen, O. K.; Sangiovanni, G.; Held, K.; Marsi, M. A Microscopic View on the Mott Transition in Chromium-doped $V_2O_3$. *Nat. Commun.* **2010**, *1*, 105.

(20) Hu, L.; Xie, C.; Zhu, S. J.; Zhu, M.; Wei, R. H.; Tang, X. W.; Lu, W. J.; Song, W. H.; Dai, J. M.; Zhang, R. R.; Zhang, C. J.; Zhu, X. B.; Sun, Y. P. Unveiling the Mechanisms of Metal-Insulator Transitions in $V_2O_3$: The Role of Trigonal Distortion. *Phys. Rev. B* **2021**, *103*, 085119.

(21) Homm, P.; Menghini, M.; Seo, J. W.; Peters, S.; Locquet, J.-P. Room Temperature Mott Metal−Insulator Transition in $V_2O_3$ Compounds Induced via Strain-Engineering. *Apl. Mater.* **2021**, *9*, 021116.

(22) Müller, O.; Urbach, J. P.; Goering, E.; Weber, T.; Barth, R.; Schuler, H.; Klemm, M.; Horn, S.; DenBoer, M. L. Spectroscopy of Metallic and Insulating V 2 O 3. *Phys. Rev. B: Condens. Matter Mater. Phys.* **1997**, *56*, 15056.
(23) Papalazarou, E.; Gatti, M.; Marsi, M.; Brouet, V.; Iori, F.; Reining, L.; Annese, E.; Vobornik, I.; Offi, F.; Fondacaro, A.; Huotari, S.; Lacovig, P.; Tjernberg, O.; Brookes, N. B.; Sacchi; Metcalf, P.; Panaccione, G. Valence-band Electronic Structure of V 2 O 3: Identification of V and O bands. *Phys. Rev. B: Condens. Matter Mater. Phys.* **2009**, *80*, 155115.
(24) Sun, G.; Cao, X.; Long, S.; Li, R.; Jin, P. Optical and Electrical Performance of Thermochromic $V_2O_3$ Thin film Fabricated by Magnetron Sputtering Appl. *Phys. Lett.* **2017**, *111*, 053901.
(25) Moffatt, D. M.; Runt, J. P.; Halliyal, A.; Newnham, R. E. Metal Oxide-Polymer Thermistors. *J. Mater. Sci.* **1989**, *24*, 609.
(26) Salev, P.; Valle, J.; Kalcheim, Y.; Schuller, I. K. Giant Nonvolatile Resistive Switching in a Mott oxide and Ferroelectric Hybrid. *Proc. Natl. Acad. Sci. U.S.A.* **2019**, *10*, 1073.
(27) Ronchi, A.; Franceschini, P.; Homm, P.; Gandolfi, M.; Ferrini, G.; Pagliara, S.; Banfi, F.; Menghini, M.; Locquet, J. P.; Giannetti, C. Light-Assisted Resistance Collapse in a V 2 O 3-Based Mott-Insulator Device. *Rev. Phys. Appl.* **2021**, *15*, 044023.
(28) Kalcheim, Y.; Camjayi, A.; del Valle, J.; Salev, P.; Rozenberg, M.; Schuller, I. K. Non-thermal resistive switching in Mott insulator nanowires. *Nat. Commun.* **2020**, *11*, 2985.
(29) Zaanen, J.; Sawatzky, G. A.; Allen, J. W. Band Gaps and Electronic Structure of Transition-Metal Compounds. *Phys. Rev. Lett.* **1985**, *55*, 418.
(30) Bocquet, A. E.; Mizokawa, T.; Morikawa, K.; Fujimori, A.; Barman, S. R.; Maiti, K.; Sarma, D. D.; Tokura, Y.; Onoda, M. Electronic Structure of Early 3d-Transition-Metal Oxides by Analysis of the 2p Core-level Photoemission Spectra. *Phys. Rev. B: Condens. Matter Mater. Phys.* **1996**, *53*, 1161.
(31) Peng, H. Y.; Li, Y. F.; Lin, W. N.; Wang, Y. Z.; Gao, X. Y.; Wu, T. Deterministic Conversion Between Memory and Threshold Resistive Switching via tuning the Strong Electron Correlation. *Sci. Rep.* **2012**, *2*, 442.
(32) Yamaguchi, I.; Manabe, T.; Kumagai, T.; Kondo, W.; Mizuta, S. Preparation of epitaxial V2O3 films on C-, A-and R-planes of $\alpha$-Al2O3 substrates by coating-pyrolysis process. *Thin Solid Films* **2000**, *366*, 294−301.
(33) Kurtz, R. L.; Henrich, V. E. Surface Electronic Structure and Chemisorption on Corundum Transition-Metal Oxides: V 2 O 3. *Phys. Rev. B: Condens. Matter Mater. Phys.* **1983**, *28*, 12.
(34) Mo, S.-K.; Denlinger, J. D.; Kim, H.-D.; Park, J.-H.; Allen, J. W.; Sekiyama, A.; Yamasaki, A.; Kadono, K.; Suga, S.; Saitoh, Y.; Muro, T.; Metcalf, P.; Keller, G.; Held, K.; Eyert, V.; Anisimov, V. I.; Vollhardt, D. Prominent Quasiparticle Peak in the Photoemission Spectrum of the Metallic Phase of $V_2O_3$. *Phys. Rev. Lett.* **2003**, *90*, 186403.
(35) Kotliar, G.; Vollhardt, D. Strongly correlated materials: Insights from Dynamical Mean-Field Theory. *Phys. Today* **2004**, *57*, 53.
(36) Shin, S.; Suga, S.; Taniguchi, M.; Fujisawa, M.; Kanzaki, H.; Fujimori, A.; Daimon, H.; Ueda, Y.; Kosuge, K.; Kachi, S. Vacuum-Ultraviolet Reflectance and Photoemission Study of the Metal-Insulator Phase Transitions in VO 2, V 6 O 13, and V 2 O 3. *Phys. Rev. B: Condens. Matter Mater. Phys.* **1990**, *41*, 4993.
(37) Maiti, K.; Sarma, D. D. Spectroscopic Investigations of the Electronic Structure and Metal-Insulator Transitions in a Mott-Hubbard system La 1− x Ca x VO 3. *Phys. Rev. B: Condens. Matter Mater. Phys.* **2000**, *61*, 2525.
(38) Mossanek, R. J. O.; Abbate, M. Importance of the V 3 d−O 2 p Hybridization in the Mott-Hubbard Material $V_2$ $O_3$. *Phys. Rev. B: Condens. Matter Mater. Phys.* **2007**, *75*, 115110.
(39) Smith, K. E.; Henrich, V. E. Valence-Band Structure of V2O3 (1012). *J. Vac. Sci. Technol., A* **1988**, *6*, 831.
(40) Chowdhury, S.; Jana, A.; Kuila, M.; Reddy, V. R.; Choudhary, R. J.; Phase, D. M. Negative Charge-Transfer Energy in SrCoO2. 5 Thin Films: An Interplay between O-2p Hole Density, Charge-Transfer Energy, Charge Disproportionation, and Ferromagnetic Ordering. *ACS Appl. Electron. Mater.* **2020**, *2*, 3859−3870.
(41) Masuda, S.; Aoki, M.; Harada, Y.; Hirohashi, H.; Watanabe, Y.; Sakisaka, Y.; Kato, H. Observation of Anomalously Enhanced Satellite in Metastable Atom Electron Spectrum of LaCoO 3. *Phys. Rev. Lett.* **1993**, *71*, 4214.
(42) Lucovsky, G.; Vargn, A. J.; Schwarz, R. F. Edge Absorption and Photoluminescence in Closely Compensated GaAs. *Solid State Commun.* **1965**, *3*, 9.
(43) Barth, J.; Gerken, F.; Kunz, C. Experimental Study of the 3p-3d Intershell Interaction in Ca, Sc, Ti, V, and Cr metals. *Phys. Rev. B: Condens. Matter Mater. Phys.* **1985**, *31*, 2022.
(44) Smith, K. E.; Henrich, V. E. Bulk Band Dispersion in Ti 2 O 3 and V 2 O 3. *Phys. Rev. B: Condens. Matter Mater. Phys.* **1988**, *38*, 35965.
(45) McKay, J. M.; Mohamed, M. H.; Henrich, V. E. Localized 3p Excitations in 3d Transition-Metal-Series Spectroscopy. *Phys. Rev. B: Condens. Matter Mater. Phys.* **1987**, *35*, 4304.
(46) Pen, H. F.; Abbate, M.; Fuijmori, A.; Tokura, Y.; Eisaki, H.; Uchida, S.; Sawatzky, G. A. Electronic Structure of Y 1− x Ca x VO 3 studied by High-Energy Spectroscopies. *Phys. Rev. B: Condens. Matter Mater. Phys.* **1999**, *59*, 7422.
(47) de Groot, F. M. F.; Fuggle, J. C.; Thole, B. T.; Sawatzky, G. A. 2p X-ray Absorption of 3d Transition-Metal Compounds: An Atomic Multiplet Description including the Crystal Field. *Phys. Rev. B: Condens. Matter Mater. Phys.* **1990**, *42*, 5459.
(48) Zaanen, J.; Sawatzky, G. A.; Fink, J.; Speier, W.; Fuggle, J. C. L 2, 3 Absorption Spectra of the Lighter 3d Transition Metals. *Phys. Rev. B: Condens. Matter Mater. Phys.* **1985**, *32*, 4905.
(49) Abbate, M.; Pen, H.; Czyżyk, M. T.; de Groot, F. M. F.; Fuggle, J. C.; Ma, Y. J.; Chen, C. T.; Sette, F.; Fujimori, A.; Ueda, Y.; Kosuge, k. Soft X-ray Absorption Spectroscopy of Vanadium Oxides. *J. Electron Spectrosc. Relat. Phenom.* **1993**, *62*, 185−195.
(50) Haskel, D.; Islam, Z.; Lang, J.; Kmety, C.; Srajer, G.; Pokhodnya, K. I.; Epstein, A. J.; Miller, J. S. Local structural order in the disordered vanadium tetracyanoethylene room-temperature molecule-based magnet. *Phys. Rev. B: Condens. Matter Mater. Phys.* **2004**, *70*, 054422.
(51) Nomura, K. Solution X-ray absorption spectroscopy (XAS) for analysis of catalytically active species in reactions with ethylene by homogeneous (imido) vanadium (V) complexes-Al cocatalyst systems. *Catalysts* **2019**, *9*, 1016.
(52) Rata, A. D.; Chezan, A. R.; Haverkort, M. W.; Hsieh, H. H.; Lin, H. J.; Chen, C. T.; Tjeng, L. H.; Hibma, T. Growth and properties of strained VO x thin films with controlled stoichiometry. *Phys. Rev. B: Condens. Matter Mater. Phys.* **2004**, *69*, 075404.
(53) Park, J.-H.; Tjeng, L. H.; Tanaka, A.; Allen, J. W.; Chen, C. T.; Metcalf, P.; Honig, J. M.; de Groot, F. M. F.; Sawatzky, G. A. Spin and orbital occupation and phase transitions in V2O3. *Phys. Rev. B: Condens. Matter Mater. Phys.* **2000**, *61*, 11506.
(54) Majid, S. S.; Shukla, D. K.; Rahman, F.; Gautam, K.; Choudhary, R. J.; Sathe, V. G.; Phase, D. M. Stabilization of Metallic Phase in V2O3 Thin film. *Appl. Phys. Lett.* **2017**, *110*, 173101.
(55) Harrison, W. A. *Electronic Structure and Physical Properties of Solids*; Freeman: San Francisco, 1980.
(56) Jana, A.; Choudhary, R. J.; Phase, D. M. Mott-Hubbard type Insulating Nature of Epitaxial LaVO3 Thin films. *Phys. Rev. B* **2018**, *98*, 075124.
(57) Wadati, H.; Hotta, Y.; Fujimori, A.; Susaki, T.; Hwang, H. Y.; Takata, Y.; Horiba, K.; Matsunami, M.; Shin, S.; Yabashi, M.; Tamasaku, K.; Nishino, Y.; Ishikawa, T. Hard X-ray Photoemission Study of La Al O 3/ La V O 3 Multilayers. *Phys. Rev. B: Condens. Matter Mater. Phys.* **2008**, *77*, 045122.
(58) Stavitski, E.; de Groot, F. M. F. The CTM4XAS Program for EELS and XAS Spectral Shape Analysis of Transition Metal L edge. *Micron* **2010**, *41*, 687−694.
(59) Newnham, E. E.; Haan, Y. M. D. Refinement of the a Al2O3, Ti2O3, V2O3 and Cr2O3 Structures. *Z. für Kristallogr.—Cryst. Mater.* **1962**, *117*, 235−237.


https://doi.org/10.1021/acsaelm.2c00460
ACS Appl. Electron. Mater. 2022, 4, 3036−3048

(60) Chen, S.; Hahn, J. E.; Rice, C. E.; Robinson, W. R. The Effects of Titanium or Chromium Doping on the Crystal Structure of V2O3. *J. Solid State Chem.* **1982**, *44*, 192−200.
(61) Zhao, H. J.; Ren, W.; Chen, X. M.; Bellaiche, L. Effect of Chemical Pressure, Misfit Strain and Hydrostatic Pressure on Structural and Magnetic Behaviors of Rare-Earth Orthochromates. *J. Phys.: Condens. Matter* **20013**, *25*, 385604.
(62) Rozenberg, M. J.; Kotliar, G.; Kajueter, H. Transfer of Spectral Weight in Spectroscopies of Correlated Electron Systems. *Phys. Rev. B: Condens. Matter Mater. Phys.* **1996**, *54*, 8452.
(63) Stewart, M. K.; Brownstead, D.; Wang, S.; West, K. G.; Ramirez, J. G.; Qazilbash, M. M.; Perkins, N. B.; Schuller, I. K.; Basov, D. N. Insulator-to-Metal Transition and Correlated Metallic State of V 2 O 3 Investigated by Optical Spectroscopy. *Phys. Rev. B: Condens. Matter Mater. Phys.* **2012**, *85*, 205113.
(64) Qazilbash, M. M.; Hamlin, J. J.; Baumbach, R. E.; Zhang, L.; Singh, D. J.; Maple, M. B.; Basov, D. N. Electronic Correlations in the Iron Pnictides. *Nat. Phys.* **2009**, *5*, 647.
(65) Fujiwara, H.; Sekiyama, A.; Mo, S. K.; Allen, J. W.; Yamaguchi, J.; Funabashi, G.; Imada, S.; Metcalf, P.; Higashiya, A.; Yabashi, M.; Tamasaku, K.; Ishikawa, T.; Suga, S. Evidence for the Constancy of U in the Mott Transition of V 2 O 3. *Phys. Rev. B: Condens. Matter Mater. Phys.* **2011**, *84*, 075117.
(66) Mahana, S.; Manju, U.; Nandi, P.; Welter, E.; Priolkar, K. R.; Topwal, D. Role of local structural distortion in driving ferroelectricity in GdCrO 3. *Phys. Rev. B* **2018**, *97*, 224107.
(67) Zhi, B.; Gao, G.; Xu, H.; Chen, F.; Tan, X.; Chen, P.; Wang, L.; Wu, W. Electric-Field-Modulated Nonvolatile Resistance Switching in VO2/PMN-PT (111) Heterostructures. *ACS Appl. Mater. Interfaces* **2014**, *6*, 4603−4608.
(68) Ravel, B. ATOMS: Crystallography for the X-ray Absorption Spectroscopist. *J. Synchrotron Radiat.* **2001**, *8*, 314.





https://doi.org/10.1021/acsaelm.2c00460
*ACS Appl. Electron. Mater.* 2022, 4, 3036−3048